

Charge density waves in cuprate superconductors beyond the critical doping

H. Miao,^{1,*} G. Fabbris,² R. J. Koch,¹ D. G. Mazzone,^{1,†} C. S. Nelson,³ R. Acevedo-Esteves,³ G. D. Gu,¹ Y. Li,¹ T. Yilmaz,³ K. Kaznatcheev,³ E. Vescovo,³ M. Oda,⁴ T. Kurosawa,⁴ N. Momono,⁵ T. Assefa,¹ I. K. Robinson,^{1,6} E. S. Bozin,¹ J. M. Tranquada,¹ P. D. Johnson,¹ and M. P. M. Dean^{1,‡}

¹*Condensed Matter Physics and Materials Science Department,
Brookhaven National Laboratory, Upton, New York 11973, USA*

²*Advanced Photon Source, Argonne National Laboratory, Argonne, Illinois 60439, USA*

³*National Synchrotron Light Source II, Brookhaven National Laboratory, Upton, NY 11973, USA*

⁴*Department of Physics, Hokkaido University, Sapporo 060-0810, Japan*

⁵*Department of Sciences and Informatics, Muroran Institute of Technology, Muroran 050-8585, Japan*

⁶*London Centre for Nanotechnology, University College, Gower St., London WC1E 6BT, UK*

(Dated: February 23, 2021)

The unconventional normal-state properties of the cuprates are often discussed in terms of emergent electronic order that onsets below a putative critical doping of $x_c \approx 0.19$. Charge-density wave (CDW) correlations represent one such order; however, experimental evidence for such order generally spans a limited range of doping that falls short of the critical value x_c , leading to questions regarding its essential relevance. Here, we use x-ray diffraction to demonstrate that CDW correlations in $\text{La}_{2-x}\text{Sr}_x\text{CuO}_4$ persist up to a doping of at least $x = 0.21$. The correlations show strong changes through the superconducting transition, but no obvious discontinuity through $x_c \approx 0.19$, despite changes in Fermi surface topology and electronic transport at this doping. These results demonstrate the interaction between CDWs and superconductivity even in overdoped cuprates and prompt a reconsideration of the role of CDW correlations in the high-temperature cuprate phase diagram.

INTRODUCTION

The cuprate high- T_c superconductors are often conceptualized as doped Mott insulators, in which the electronic ground state spontaneously breaks rotational and/or translational symmetry [1–4]. While cuprate CDW correlations were discovered over two decades ago [5], their possible contribution to the material’s anomalous electronic properties remains a matter of vigorous debate [1, 6–10]. This issue has gained increasing attention in light of the ubiquity of CDW order in different cuprate families [5, 11–19]. The cuprate phase diagram, shown in Fig. 1(a), shows that pseudogap, strange metal, and superconducting phases exist over an extensive doping range below a critical doping level of $x_c \approx 0.19$, above which the cuprate electronic properties become gradually more Fermi-liquid-like [20–27]. If CDW correlations are confined to underdoped cuprates, as previously suggested [11–21], that would preclude the possibility of CDW correlations having an important role in the anomalous electronic properties. For instance, it has been argued that since CDW correlations disappear at $x \ll x_c$, the quantum critical point (QCP) at $x = x_c$ must be magnetic in nature [8]. Tunneling spectroscopy studies have suggested a vestigial nematic QCP on a similar basis [28, 29]. Very recent nuclear magnetic resonance results have reported the disappearance of spin glass behavior near x_c [30]. Whether this disappearance is associated with the loss of stripe correlations (i.e. coupled spin and charge density waves) remains unresolved. Moreover, the existence of CDW correlations is also crucial for the rele-

vance of intertwined order. Many theoretical models for pair-density-wave superconducting states, for example, require the presence of CDW correlations [1, 31].

Studies of underdoped and optimally doped cuprates have shown that CDW correlations exist up to temperatures well above the nominal CDW transition temperature [32, 33]. More recently, re-entrant charge order, disconnected from the CDW at lower doping, was observed in overdoped $(\text{Bi, Pb})_{2.12}\text{Sr}_{1.88}\text{CuO}_{6+\delta}$ [19]. These results motivate a reconsideration of the cuprate phase diagram, in which CDW correlations may extend up to higher dopings than previously thought [33]. Herein, we address this issue by focusing on $\text{La}_{2-x}\text{Sr}_x\text{CuO}_4$ (LSCO) ($x = 0.12, 0.17, 0.21, \& 0.25$) single crystals in view of its particularly well characterized transport properties and the feasibility of synthesizing high-quality samples across the entire phase diagram [21, 24–27] (see Methods Section).

RESULTS

Electronic structure

Previous measurements of LSCO established the presence of a critical doping $x_c \sim 0.19$, which was defined as the doping above which the electronic transport acquires partial Fermi-liquid-like properties [21, 24]. This point coincides with, and is perhaps related to, the doping where the Fermi surface topology undergoes a Lifshitz transition [35, 36]. To prove the Sr doping, x , is consistent with previous studies, and that we indeed

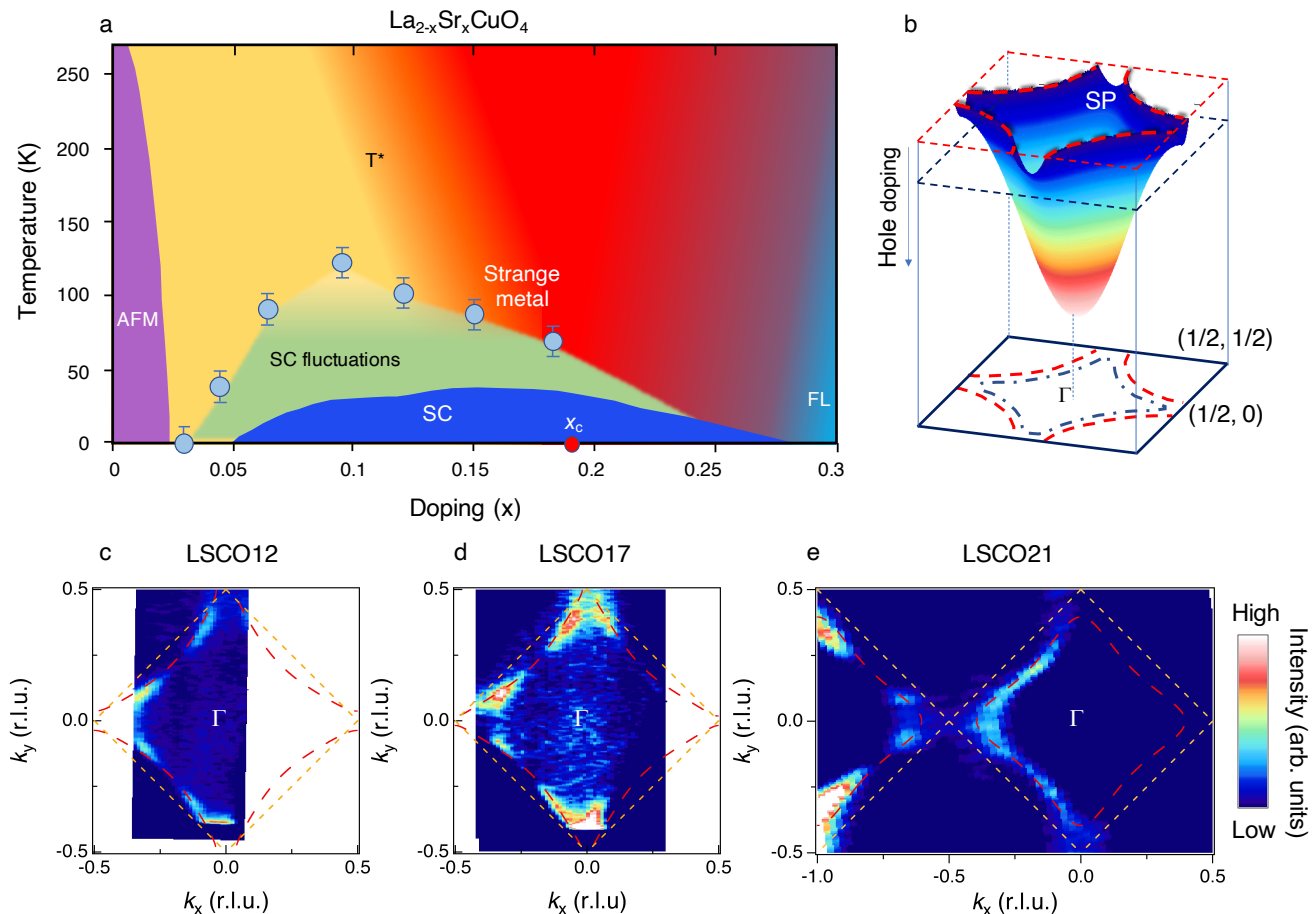


Figure 1. Doping dependent electronic structure of LSCO. (a) Phase diagram of the hole-doped cuprates, constructed from magnetization, Nernst effect and resistivity data for LSCO [20, 34]. T^* is the extracted pseudogap onset temperature [20, 34]. (b) Schematic band structure of LSCO. The Fermi energy, E_F , crosses the anti-nodal saddle-point (labeled as SP) near $x_c \approx 0.19$ triggering a Lifshitz transition. (c)-(e) Fermi surface topology of LSCO12, LSCO17 and LSCO21. The intensity plots are obtained by integrating the spectra within ± 10 meV of E_F . Orange dashes outline the antiferromagnetic Brillouin zone. Red dashed contours represent a tight-binding fit of the Fermi surface (see Supplementary note 1). The data shown in (c)-(e) were collected at 11 K.

access the $x > x_c$ region of the overdoped phase diagram, we show the electronic structure evolution with doping in Fig. 1(b)-(e). The angle-resolved photoemission spectroscopy (ARPES) methods used are described in the Methods Section. Figure 1(b) illustrating the two-dimensional electronic structure. At low doping, to the extent that a Fermi surface exists, it is hole-like and centered at the Brillouin zone corner. With increasing hole concentration, the chemical potential drops and eventually passes through the saddle point. This results in a Lifshitz transition to an electron-like Fermi surface at the Brillouin zone center. In LSCO, the saddle point is three-dimensional with small k_z dispersion. Near x_c , the saddle point coincidentally crosses the Fermi level. It should be noted that the carrier concentration determined by the Fermi surface (FS) area is significantly larger than the nominal Sr-doping. The origin of this ef-

fect remains, however, unresolved [35, 36]. Nevertheless, the well-established FS evolution in LSCO can be used to confirm the Sr-doping in this study. Figure 1(c)-(e) shows ARPES measurements for LSCO12, LSCO17, and LSCO21. An electron-like FS is observed in LSCO21, consistent with $x_c = 0.19$ and in agreement with previous ARPES studies [35, 36].

CDW order

Having confirmed the electronic structure, we now present our main experimental finding of CDW correlations beyond x_c . Figure 2 plots x-ray reciprocal space scans for LSCO21 at $T = 16$ K, where reciprocal space is defined in terms of scattering vector $\mathbf{Q} = (H, K, L)$ using effective tetragonal lattice constants $a = b \approx 3.8$ Å and

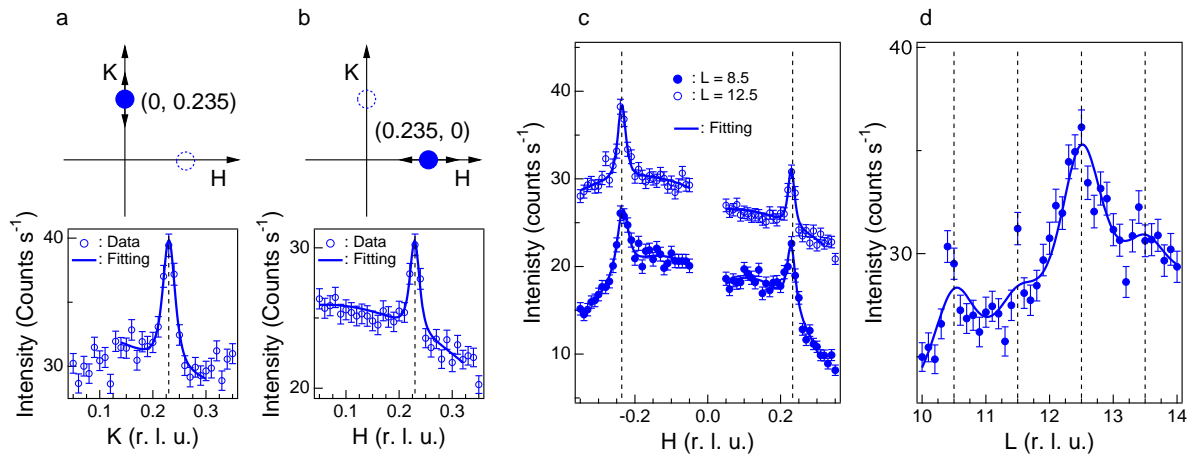


Figure 2. Discovery of a CDW beyond x_c . (a) & (b) X-ray diffraction measurements of LSCO21 at $T = 16$ K along $(0, K, 12.5)$ and $(H, 0, 12.5)$. Supperlattice peaks are observed at $(0, 0.235, 12.5)$ and $(0.235, 0, 12.5)$. The H -scans in (c) reveal further CDW peaks at $(\pm 0.235, 0, L)$ for $L = 8.5$ and 12.5 . The data at $L = 8.5$ are offset by -10 counts s^{-1} for visibility. (d) The L -dependence of the intensity along $(-0.235, 0, L)$ demonstrates poorly correlated out-of-phase CDW stacking along the c -axis. Solid lines are fits to the experimental data as described in the text and Supplementary note 2. Errorbars are one standard deviation based on Poissonian statistics.

$c \approx 13.2$ Å. High sensitivity is achieved by exploiting the high brightness of the National Synchrotron Light Source II and by careful configuration of the detection system to suppress background signal (see Methods Section). Supperlattice peaks are observed at $(0.235, 0, 12.5)$, and equivalent locations, along both the H and K directions [Fig. 2 (a)&(b)]. The observed $H = 0.235$ matches the CDW wavevector in underdoped LSCO [16–18, 37] and is consistent with the charge stripe picture [5]. The peaks are symmetric with respect to $\pm H$ and K and are observed in multiple Brillouin zones including $(\pm 0.235, 0, L)$ for $L = 8.5$ & 12.5 . An L -scan along $\mathbf{Q} = (-0.235, 0, L)$ [Fig. 2(d)] reveals that the CDW intensity is broadly peaked at half-integer L similar to underdoped LSCO [17, 18, 38]. These results demonstrate the presence of CDW correlations beyond x_c . Subsequent inelastic x-ray scattering studies show that the CDW is associated with phonon softening even in the overdoped regime [39].

CDW temperature dependence

Figure 3 summarizes the doping and temperature dependence of the CDW correlations. In Fig. 3(a), Lorentzian-squared fits to the data are shown, which are parameterized in terms of amplitude, $I_{\text{CDW}}(T)$, and in-plane correlation length, $\xi_{\parallel}(T) = 1/\text{HWHM}$ (where HWHM is half-width at half-maximum) (see Supplementary note 2). Since domain formation can lead to transverse peak splitting in LSCO [c.f. Refs. [16, 18, 37] and Fig. 3(a)], we scanned through the peaks in all three reciprocal space directions. Two Lorentzian-squared functions displaced in the K (transverse) direction were used, where necessary, to account for the full intensity dis-

tribution. Peak widths and correlation lengths are determined using the H (longitudinal) cut. $I_{\text{CDW}}(T)$ is found to be largest near T_{SC} for all dopings [Fig. 3(b)]. Above T_{SC} , both I_{CDW} and $\xi_{\parallel}(T)$ decrease with increasing temperature but remain finite up to at least $T = 90$ K [Fig. 3(a)]. In agreement with previous x-ray diffraction studies of LSCO [16, 17, 37], the correlation length can be separated into a marginally-ordered regime where $\xi_{\parallel}(T)$ is approximately 4-unit-cells (about one period of the CDW order), and a strongly T -dependent regime where $\xi_{\parallel}(T)$ continues to expand until superconductivity intervenes. We refer to the CDW in the T -independent regime as “precursor” CDW correlations in the sense that they come before the emergence of a stronger, more-correlated CDW at low temperatures. Note that for these measurements we do not have the energy resolution to directly distinguish between dynamic and static correlations. The short correlation length and quasi-temperature-independent nature of the precursor CDW indicates that it might be dynamic in nature. This phenomenology is consistent with resonant inelastic x-ray scattering (RIXS) scattering studies of $\text{La}_{2-x}\text{Ba}_x\text{CuO}_4$ (LBCO x) and $\text{YBa}_2\text{Cu}_3\text{O}_{6+\delta}$ which show a similar two-stage CDW formation [32, 33, 40, 41]. While the CDW evolves smoothly from LSCO12 to LSCO21, both ξ_{\parallel} and the onset temperature of the longer-range CDW, T_{ξ} , are suppressed in the overdoped regime around x_c [Fig. 3(c) and Fig. 4]. The \mathbf{Q} -integrated scattering intensity, as estimated by $I_{\text{CDW}}\xi_{\parallel}^2$, shows minimal variation through T_{SC} , indicating that while superconductivity alters the CDW correlation length, it does not strongly suppress the order parameter. We do not observe any CDW correlations in our high-sensitivity x-ray measurements at

$x = 0.25$ (see Supplementary note 3).

Previous measurements of the same $x = 0.12$ sample allow us to compare the CDW order parameter, taken to be captured by the total \mathbf{Q} -integrated scattering intensity, to other cuprate systems [16]. The CDW order parameter of LSCO12 is only four times weaker than $\text{La}_{1.875}\text{Ba}_{0.125}\text{CuO}_4$ (which has the strongest zero-field CDW order). With increasing doping, the LSCO CDW becomes somewhat stronger for $x = 0.17$ and drops appreciably for $x = 0.21$ (see Supplementary note 4). Consequently, CDW correlations can have an appreciable effect on the physics of LSCO x for dopings through x_c .

DISCUSSION

Figure 4 summarizes our main observations – that CDW correlations exist far into the overdoped regime of the cuprate phase diagram. This immediately yields three important consequences for LSCO. Firstly, very similar CDW properties that are observed either side of the Lifshitz transition. This provides a vivid demonstration that CDW correlations cannot be explained within a weak coupling Fermi surface nesting picture nor Friedel oscillations. Instead, the nearly constant \mathbf{Q}_{CDW} for dopings $x \geq 0.125$ support strong coupling mechanisms, which date back to seminal work in the late 1980s [2–4]. In these mechanisms one considers the balance between Coulomb interactions and kinetic energy. When doping a Mott insulator holes can save energy by clustering together as this breaks fewer magnetic bonds than widely dispersed holes. At the same time, this clustering is disfavored by the increased Coulomb repulsion and kinetic energy reduction. Since these different interactions act on different lengthscales, the overall minimum energy solution is expected to involve a spatially modulated state. Modern numerical solutions of the Hubbard model further support this idea [42–44] and models based on filled stripes can reproduce a doping-independent CDW wavevector from $x = 1/8$ to $x = 1/4$ [45]. We also note that precursor CDW correlations are emerging as a ubiquitous feature for many cuprates, including LSCO in this study, underdoped LBCO [41], underdoped and optimally doped YBCO [33], underdoped Bi2212 [46] and $\text{HgBa}_2\text{CuO}_{4+\delta}$ [47]. In underdoped and optimally doped YBCO, the precursor correlations appear to exist at the same wavevector around 0.3 r.l.u. different to the doping-dependent low-temperature CDW [33]. It would consequently be interesting to consider a possible role for strong coupling mechanisms for all cuprates. An obviously desirable experiment would be to test whether other cuprates, such as YBCO, also exhibit CDW correlations up to similarly high dopings as LSCO. Such experiments are, however, currently held back by challenges in stabilizing high-quality heavily overdoped YBCO crystals. The robust presence of CDW correlations in LSCO

seen here as a function of temperature and doping, as well as the fact that model Hamiltonian calculations reliably predict CDW correlations [42–44], would point towards their likely presence. The issue of differing wavevectors in different cuprates would, however, not necessarily be solved by such an experiment. In this regard, it is important to point out the low-temperature ordering wavevector can be influenced by coupling between the CDW and spin correlations or coupling between the CDW and the lattice, as has been suggested theoretically [48], so differences in CDW wavevectors could arise from secondary interactions rather than necessarily indicating a distinct origin for the correlations. Prior work has pointed towards this as a possible explanation for temperature-induced changes in CDW wavevector in LBCO [32].

A second immediate conclusion is that the continuous evolution of the CDW correlations is inconsistent with the proposed QCP that is associated with x_c arising from CDW or coupled CDW/spin-density wave (SDW) order [6, 10]. Such theories can still be excluded even if one postulates a very narrow range of criticality around x_c , since they require either a disappearance or a symmetry change of the CDW through x_c .

Last but not least, the disappearance of CDW in LSCO25 suggests that the CDW dome in LSCO terminates between $x = 0.21$ and 0.25 , where the Fermi liquid behavior starts to recover [21, 24, 25]. This is, again, consistent with a strong coupling CDW mechanism as Coulomb repulsion is largely screened in the Fermi liquid state. We note that in LSCO, the structural high-temperature tetragonal to low-temperature orthorhombic (LTO) phase transition also terminates near $x = 0.21$ [49]. It has been argued that the local LTO distortion may help to stabilize the CDW [50]. The persistence of CDW correlations up to $x = 0.21$ observed in this study is consistent with this scenario and indicates that electron-phonon coupling might be an important ingredient for the CDW formation [39, 40].

The observations herein also urge a re-examination of the potential role of CDWs in the anomalous electronic properties of the cuprates. CDW correlations are a prerequisite (but not a proof) of several prominent theories of cuprate properties, which would be expected to apply across the phase diagram and not just in the underdoped region where CDW correlations have been studied extensively in the past. This includes the possibility that CDW correlations play a key role in the electronic transport properties [6, 10]. Theories of pair-density-wave order [1, 31, 51, 52], which predict competition between the CDW and uniform d -wave superconductivity, also fall into this category. As shown in Fig. 3, neither the CDW peak intensity nor the CDW correlation length show the type of divergent-behavior associated with a typical phase transition. This behavior is consistent with a possible fluctuating CDW component, potentially influencing cuprate transport properties [24–27, 33].

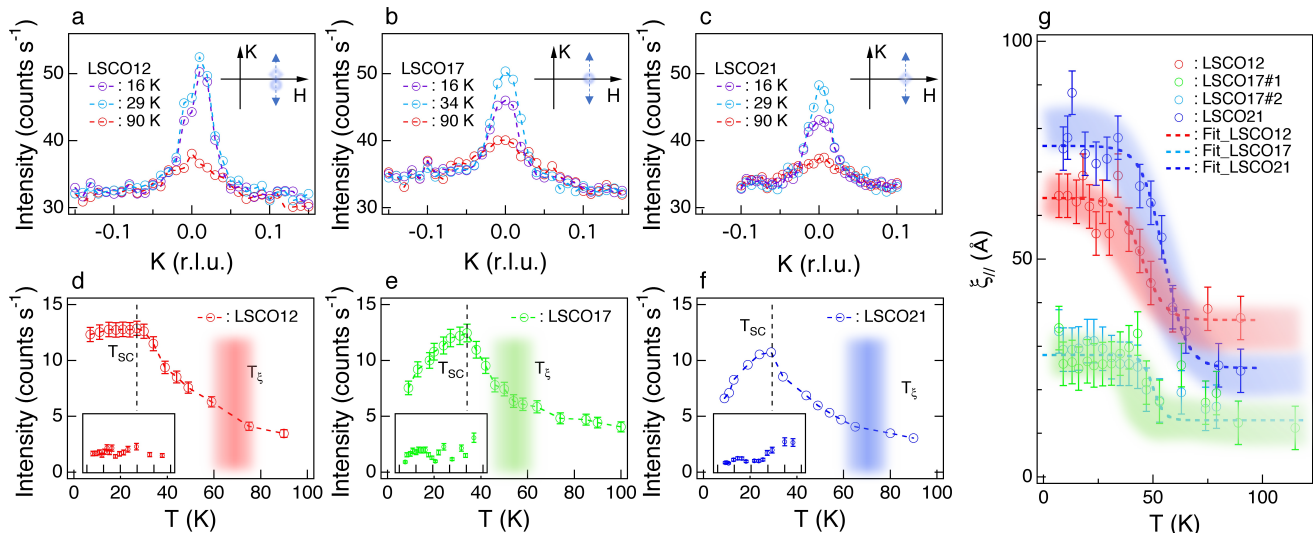


Figure 3. CDW temperature dependence. (a)-(c) Doping dependence of the CDW peak intensity for temperatures $T < T_{\text{SC}}$, $T \approx T_{\text{SC}}$, and $T > T_{\text{SC}}$ for (a) LSCO12, (b) LSCO17, and (c) LSCO21. The inset of each panel represents the respective cut in reciprocal space. All data were taken at $L = 8.5$ (d)-(f) Temperature dependence of the CDW intensity in LSCO for (d) LSCO12, (e) LSCO17, and (f) LSCO21. The shaded area corresponds to T_{ξ} where the in-plane CDW correlation length, ξ_{\parallel} , starts to increase [as determined in (g)]. The main panels show peak height intensity and the insets show integrated intensity. (g) Temperature dependence of ξ_{\parallel} . The colored shaded curves are phenomenological fittings, $a + \frac{b}{1 + e^{(T-T_0)/4\Delta T}}$, of the temperature dependent ξ_{\parallel} for different dopings. Here we define $T_{\xi} = T_0 + \Delta T$. ξ_{\parallel} increases with decreasing temperature for $T_{\text{SC}} < T < T_{\xi}$. Two independent measurements of LSCO17 samples at different beamlines show consistent suppression of ξ_{\parallel} and T_{ξ} , indicating that systematic errors are minimal. Due to the short correlation length, the uncertainty of T_{ξ} may be larger in LSCO17 than other dopings. Errorbars are one standard deviation from either Poissonian statistics or least-squares fitting.

Finally, we note that a charge Bragg peak has recently been observed in overdoped $(\text{Bi,Pb})_{2.12}\text{Sr}_{1.88}\text{CuO}_{6+\delta}$ (Bi2201), with a maximum doping comparable to that observed here [19]. This state, termed re-entrant charge order, has several properties that are different to CDW states in LSCO and other cuprates. Re-entrant charge order appears to exist only in an isolated region of the overdoped phase diagram, disconnected from the underdoped CDW order. The correlation length and temperature scale of this state are also far higher than other cuprates. Intriguingly, no interaction between re-entrant charge order and superconductivity is observed in Bi2201. In contrast, similarly well-correlated CDW states are associated with a strong suppression of superconductivity. All these behaviors are in strong contrast with the CDW in overdoped LSCO, where the CDW wavevectors, correlation length and temperature dependence evolve smoothly from the properties of underdoped LSCO and strongly intertwine with superconductivity and low-temperature transport. Based on the electronic structure of Bi2201 and the wavevector of re-entrant charge order around 0.1 r.l.u., which extrapolates roughly linearly from the underdoped CDW wavevector, re-entrant charge order was proposed to arise from a van Hove singularity [19]. The overdoped CDW in LSCO appears to have no connection to this mechanism, since the CDW remains un-

changed regardless of the proximity to the van Hove singularity at $x = x_c$. Instead, our observations support strong coupling mechanisms.

In summary, high-sensitivity x-ray measurements have revealed that cuprate CDW correlations persist across almost the whole cuprate doping phase diagram, despite dramatic changes in the transport properties and Fermi surface topology, before disappearing when Fermi-liquid-like properties are restored. We have shown that these correlations impact superconductivity even in overdoped cuprates, suggesting that CDW correlations can have a far more extensive role in the cuprate phase diagram than previously envisaged, prompting investigations of CDW correlations in other overdoped cuprates. The discovery of CDWs beyond x_c is confirmed by subsequent resonant inelastic x-ray scattering studies, which uncovered an unusual coupling between the CDW and lattice vibrations [39].

METHODS

Samples

Single crystals of $\text{La}_{2-x}\text{Sr}_x\text{CuO}_4$ ($x = 0.12, 0.17, 0.21$ and 0.25) were grown by the traveling-solvent floating-

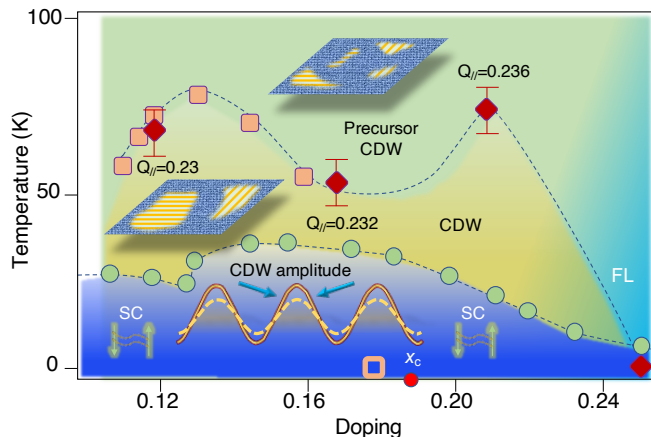


Figure 4. Illustration of the extent of CDW correlations in the cuprate phase diagram suggested by this work. Green-yellow tones represent our main result – the presence of CDW correlations, from $0.12 < x < 0.21$. Green denotes the precursor CDW, which appear at high temperature and which have a correlation length of approximately one CDW period [32, 33, 40, 41]. At lower temperature, the correlations start to grow into larger CDW domains, as evidenced by the increased correlation length, which we denote by the yellow tone. Red points mark where the correlation length starts to increase. This should be considered an approximate cross-over and not over-interpreted as a well-defined phase transition. At lower temperatures still, bulk d -wave superconductivity intervenes at T_{SC} whereupon both the CDW amplitude and the correlation length saturate or start to decrease. The doping dependence reveals an anticorrelation between T_{ξ} and T_{SC} , providing evidence for an interaction between the CDW and superconductivity. This is illustrated by the cartoon in the bottom of the diagram in which superconducting pairing (green spin pairs) suppress the CDW (yellow solid and dashed sinusoidal curves). The CDW intensity disappears in heavily overdoped LSCO25, where a Fermi-liquid-like state is recovered (Supplementary note 3 & 5). The red diamonds reflect the present study. Pink squares and green circles are data from previous work [16, 17, 34, 37].

zone method. For each composition, a single feed rod 20 – 25 cm long was used, the first few centimeters of which was removed and discarded after growth. The remaining rod was annealed in flowing O_2 at $980^{\circ}C$ for 1 week. The superconducting transition temperatures, 28, 37, 30 and 10 K were determined by dc magnetization measurements in an applied field of 1 mT (after cooling in zero field). Our tight-binding fits to our ARPES measurements of these samples, described in Supplementary note 1, confirm the hole concentration matches the strontium content x .

ARPES

ARPES measurements were performed at the 21-ID-1 beamline of the National Synchrotron Light Source II

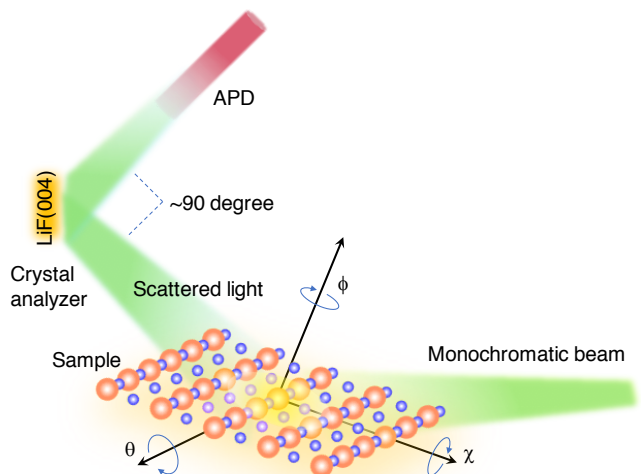


Figure 5. Illustration of the experimental geometry at the 4-ID beamline of NSLS-II.

(NSLS-II) using a Scienta-DA30 analyzer. Due to the small incident beam spot-size (less than $10 \times 10 \mu m^2$), both the sample position and the incident light angle are fixed during the measurement. The ARPES intensity maps are obtained using the mapping-mode of the DA30-analyzer, which can cover 30° of cone acceptance without sample rotation. All samples were cleaved in-situ and measured at 11 K within a vacuum better than 7×10^{-11} mbar. The photon energy was set to 60 eV for LSCO12 and LSCO17 with 18 meV energy resolution. To confirm the Fermi surface of LSCO21 is a closed loop at the Γ point, we set the photon energy to 195 eV for LSCO21 with 90 meV energy resolution. At this energy, we were able to cover the second Brillouin zone without sample rotation. The chemical potential is calibrated based on the ARPES spectra on Silver that are recorded before and after the ARPES measurement.

Non-resonant hard x-ray scattering

High-precision x-ray scattering measurements were performed at the In-situ and Resonant (ISR) 4-ID beamline of NSLS-II and 4-ID-D beamline of the Advanced Photon Source (APS). The incident photon energy was set to 8.98 keV; slightly below the Cu K -edge to minimize the fluorescence background. The measurements at NSLS-II were carried out with an avalanche photodiode (APD) detector. A LiF(004) crystal analyzer was used to further suppress the background signal (Fig. 5). The measurements at the APS used a Vortex Si drift detector without any crystal analyzer.

DATA AVAILABILITY

Data are available from the corresponding author upon reasonable request.

We thank N. Christensen, G. Kotliar, J. Q. Lin, V. Thampy, A. Tsvetik and W. G. Yin for insightful discussions, and J. Jiang and S. S. Zhang for technical support. This material is based upon work supported by the U.S. Department of Energy (DOE), Office of Basic Energy Sciences. Work at Brookhaven National Laboratory was supported by the U.S. Department of Energy, Office of Basic Energy Sciences, under Contract No. DESC0012704. X-ray and photoemission measurements used resources at the 4-ID and 21-ID-1 beamlines of the National Synchrotron Light Source II, a U.S. Department of Energy Office of Science User Facility operated for the DOE Office of Science by Brookhaven National Laboratory under Contract no. DE-SC0012704. Additional x-ray measurements used resources at 4-ID-D in the Advanced Photon Source, a U.S. Department of Energy (DOE) Office of Science User Facility operated for the DOE Office of Science by Argonne National Laboratory under Contract No. DE-AC02-06CH11357.

COMPETING INTERESTS

The authors declare no competing interests.

AUTHOR CONTRIBUTIONS

H.M., T.Y., K.K., E.V., and P.D.J. performed the ARPES measurements. H.M., G.F., R.J.K., D.G.M., C.S.N., R. A.-E., T.A., I.K.R., E.S.B., and M.P.M.D. performed the x-ray measurements. Y.L., G.D.G., M.O., K.K., and N.M. grew the LSCO samples and characterized their transport properties. H.M., P.D.J., and M.P.M.D. analyzed the data. H.M., J.M.T., and M.P.M.D. wrote the paper.

* hmiao@bnl.gov

† Present address: Laboratory for Neutron Scattering and Imaging, Paul Scherrer Institut, 5232 Villigen PSI, Switzerland

‡ mdean@bnl.gov

- [1] Fradkin, E., Kivelson, S. A. & Tranquada, J. M. *Colloquium: Theory of intertwined orders in high temperature superconductors*. *Rev. Mod. Phys.* **87**, 457–482 (2015).
- [2] Zaanen, J. & Gunnarsson, O. Charged magnetic domain lines and the magnetism of high- T_c oxides. *Phys. Rev. B* **40**, 7391–7394 (1989).
- [3] Machida, K. Magnetism in La_2CuO_4 based compounds. *Physica C Supercond.* **158**, 192–196 (1989).
- [4] Emery, V. J., Kivelson, S. A. & Lin, H. Q. Phase separation in the $t - J$ model. *Phys. Rev. Lett.* **64**, 475–478 (1990).
- [5] Tranquada, J., Sternlieb, B., Axe, J., Nakamura, Y. & Uchida, S. Evidence for stripe correlations of spins and holes in copper oxide superconductors. *Nature* **375**, 561–563 (1995).
- [6] Castellani, C., Di Castro, C. & Grilli, M. Singular quasi-particle scattering in the proximity of charge instabilities. *Phys. Rev. Lett.* **75**, 4650–4653 (1995).
- [7] Sachdev, S. Where is the quantum critical point in the cuprate superconductors? *Phys. status solidi B* **247**, 537–543 (2010).
- [8] Doiron-Leyraud, N. & Taillefer, L. Quantum critical point for stripe order: An organizing principle of cuprate superconductivity. *Physica C Supercond.* **481**, 161–167 (2012).
- [9] Sebastian, S. E. & Proust, C. Quantum oscillations in hole-doped cuprates. *Annu. Rev. Condens. Matter Phys.* **6**, 411–430 (2015).
- [10] Caprara, S., Di Castro, C., Seibold, G. & Grilli, M. Dynamical charge density waves rule the phase diagram of cuprates. *Phys. Rev. B* **95**, 224511 (2017).
- [11] Hoffman, J. *et al.* A four unit cell periodic pattern of quasi-particle states surrounding vortex cores in $\text{Bi}_2\text{Sr}_2\text{CaCu}_2\text{O}_{8+\delta}$. *Science* **295**, 466–469 (2002).
- [12] Howald, C., Eisaki, H., Kaneko, N. & Kapitulnik, A. Coexistence of periodic modulation of quasiparticle states and superconductivity in $\text{Bi}_2\text{Sr}_2\text{CaCu}_2\text{O}_{8+\delta}$. *Proc. Natl. Acad. Sci. U.S.A.* **100**, 9705–9709 (2003).
- [13] Ghiringhelli, G. *et al.* Long-range incommensurate charge fluctuations in $(\text{Y,Nd})\text{Ba}_2\text{Cu}_3\text{O}_{6+x}$. *Science* **337**, 821–825 (2012).
- [14] Comin, R. *et al.* Charge order driven by Fermi-arc instability in $\text{Bi}_2\text{Sr}_{2-x}\text{La}_x\text{CuO}_{6+\delta}$. *Science* **343**, 390–392 (2014).
- [15] Tabis, W. *et al.* Charge order and its connection with Fermi-liquid charge transport in a pristine high- T_c cuprate. *Nat. Commun.* **5**, 5875 (2014).
- [16] Thampy, V. *et al.* Rotated stripe order and its competition with superconductivity in $\text{La}_{1.88}\text{Sr}_{0.12}\text{CuO}_4$. *Phys. Rev. B* **90**, 100510 (2014).
- [17] Croft, T. P., Lester, C., Senn, M. S., Bombardi, A. & Hayden, S. M. Charge density wave fluctuations in $\text{La}_{2-x}\text{Sr}_x\text{CuO}_4$ and their competition with superconductivity. *Phys. Rev. B* **89**, 224513 (2014).
- [18] Christensen, N. B. *et al.* Bulk charge stripe order competing with superconductivity in $\text{La}_{2-x}\text{Sr}_x\text{CuO}_4$ ($x = 0.12$) Preprint at <https://arxiv.org/abs/1404.3192> (2014).
- [19] Peng, Y. *et al.* Re-entrant charge order in overdoped $(\text{Bi, Pb})_{2.12}\text{Sr}_{1.88}\text{CuO}_{6+\delta}$ outside the pseudogap regime. *Nat. Mater.* **17**, 697–702 (2018).
- [20] Wang, Y., Li, L. & Ong, N. P. Nernst effect in high- T_c superconductors. *Phys. Rev. B* **73**, 024510 (2006).
- [21] Cooper, R. A. *et al.* Anomalous criticality in the electrical resistivity of $\text{La}_{2-x}\text{Sr}_x\text{CuO}_4$. *Science* **323**, 603–607 (2009).
- [22] Keimer, B., Kivelson, S., Norman, M., Uchida, S. & Zaanen, J. From quantum matter to high-temperature superconductivity in copper oxides. *Nature* **518**, 179–186 (2015).
- [23] Ramshaw, B. J. *et al.* Quasiparticle mass enhancement approaching optimal doping in a high- T_c superconductor. *Science* **348**, 317–320 (2015).

- [24] Badoux, S. *et al.* Critical doping for the onset of Fermi-surface reconstruction by charge-density-wave order in the cuprate superconductor $\text{La}_{2-x}\text{Sr}_x\text{CuO}_4$. *Phys. Rev. X* **6**, 021004 (2016).
- [25] Giraldo-Gallo, P. *et al.* Scale-invariant magnetoresistance in a cuprate superconductor. *Science* **361**, 479–481 (2018).
- [26] Boebinger, G. S. *et al.* Insulator-to-metal crossover in the normal state of $\text{La}_{2-x}\text{Sr}_x\text{CuO}_4$ near optimum doping. *Phys. Rev. Lett.* **77**, 5417–5420 (1996).
- [27] Michon, B. *et al.* Thermodynamic signatures of quantum criticality in cuprate superconductors. *Nature* **567**, 218–222 (2019).
- [28] Nie, L., Tarjus, G. & Kivelson, S. A. Quenched disorder and vestigial nematicity in the pseudogap regime of the cuprates. *Proc. Natl. Acad. Sci. U.S.A.* **111**, 7980–7985 (2014).
- [29] Mukhopadhyay, S. *et al.* Evidence for a vestigial nematic state in the cuprate pseudogap phase. *Proc. Natl. Acad. Sci. U.S.A.* **116**, 13249–13254 (2019).
- [30] Frachet, M. *et al.* Hidden magnetism at the pseudogap critical point of a cuprate superconductor. *Nat. Phys.* **16**, 1064–1068 (2020).
- [31] Agterberg, D. F. *et al.* The physics of pair-density waves: Cuprate superconductors and beyond. *Annu. Rev. Condens. Matter Phys.* **11**, 231–270 (2020).
- [32] Miao, H. *et al.* High-temperature charge density wave correlations in $\text{La}_{1.875}\text{Ba}_{0.125}\text{CuO}_4$ without spin-charge locking. *Proc. Natl. Acad. Sci. U.S.A.* **114**, 12430–12435 (2017).
- [33] Arpaia, R. *et al.* Dynamical charge density fluctuations pervading the phase diagram of a Cu-based high- T_c superconductor. *Science* **365**, 906–910 (2019).
- [34] Yamada, K. *et al.* Doping dependence of the spatially modulated dynamical spin correlations and the superconducting-transition temperature in $\text{La}_{2-x}\text{Sr}_x\text{CuO}_4$. *Phys. Rev. B* **57**, 6165–6172 (1998).
- [35] Yoshida, T. *et al.* Systematic doping evolution of the underlying Fermi surface of $\text{La}_{2-x}\text{Sr}_x\text{CuO}_4$. *Phys. Rev. B* **74**, 224510 (2006).
- [36] Horio, M. *et al.* Three-dimensional Fermi surface of overdoped La-based cuprates. *Phys. Rev. Lett.* **121**, 077004 (2018).
- [37] Wen, J.-J. *et al.* Observation of two types of charge-density-wave orders in superconducting $\text{La}_{2-x}\text{Sr}_x\text{CuO}_4$. *Nat. Commun.* **10**, 3269 (2019).
- [38] Thampy, V. *et al.* Comparison of charge modulations in $\text{La}_{1.875}\text{Ba}_{0.125}\text{CuO}_4$ and $\text{YBa}_2\text{Cu}_3\text{O}_{6.6}$. *Phys. Rev. B* **88**, 024505 (2013).
- [39] Lin, J. Q. *et al.* Strongly correlated charge density wave in $\text{La}_{2-x}\text{Sr}_x\text{CuO}_4$ evidenced by doping-dependent phonon anomaly. *Phys. Rev. Lett.* **124**, 207005 (2020).
- [40] Miao, H. *et al.* Incommensurate phonon anomaly and the nature of charge density waves in cuprates. *Phys. Rev. X* **8**, 011008 (2018).
- [41] Miao, H. *et al.* Formation of incommensurate charge density waves in cuprates. *Phys. Rev. X* **9**, 031042 (2019).
- [42] Corboz, P., Rice, T. M. & Troyer, M. Competing states in the t - J model: Uniform d -wave state versus stripe state. *Phys. Rev. Lett.* **113**, 046402 (2014).
- [43] Huang, E. W. *et al.* Numerical evidence of fluctuating stripes in the normal state of high- T_c cuprate superconductors. *Science* **358**, 1161–1164 (2017).
- [44] Zheng, B.-X. *et al.* Stripe order in the underdoped region of the two-dimensional Hubbard model. *Science* **358**, 1155–1160 (2017).
- [45] Lorenzana, J. & Seibold, G. Metallic mean-field stripes, incommensurability, and chemical potential in cuprates. *Phys. Rev. Lett.* **89**, 136401 (2002).
- [46] Chaix, L. *et al.* Dispersive charge density wave excitations in $\text{Bi}_2\text{Sr}_2\text{CaCu}_2\text{O}_{8+\delta}$. *Nat. Phys.* **13**, 952 (2017).
- [47] Yu, B. *et al.* Unusual dynamic charge correlations in simple-tetragonal $\text{HgBa}_2\text{CuO}_{4+\delta}$. *Phys. Rev. X* **10**, 021059 (2020).
- [48] Zachar, O., Kivelson, S. A. & Emery, V. J. Landau theory of stripe phases in cuprates and nickelates. *Phys. Rev. B* **57**, 1422–1426 (1998).
- [49] Hücker, M. *et al.* Dzyaloshinsky-Moriya spin canting in the low-temperature tetragonal phase of $\text{La}_{2-x-y}\text{Eu}_y\text{Sr}_x\text{CuO}_4$. *Phys. Rev. B* **70**, 214515 (2004).
- [50] Chen, X. *et al.* Charge density wave memory in a cuprate superconductor. *Nat. Commun.* **10**, 1435 (2019).
- [51] Lee, P. A. Amperean pairing and the pseudogap phase of cuprate superconductors. *Phys. Rev. X* **4**, 031017 (2014).
- [52] Berg, E. *et al.* Dynamical layer decoupling in a stripe-ordered high- T_c superconductor. *Phys. Rev. Lett.* **99**, 127003 (2007).

Supplementary information: charge density waves in cuprate superconductors beyond the critical doping

(Dated: February 23, 2021)

SUPPLEMENTARY NOTE 1: TIGHT BINDING MODEL

The band-dispersion shown in the main text has the form [1, 2]

$$\begin{aligned} \epsilon_k = & \mu - 2t[\cos(k_x a) + \cos(k_y a)] - 4t_1 \cos(k_x a) \cos(k_y a) \\ & - 2t_2[\cos(2k_x a) + \cos(2k_y a)] - 4t_3[\cos(2k_x a) \cos(k_y a) \\ & + \cos(k_x a) \cos(2k_y a)] - 4t_4 \cos(2k_x a) \cos(2k_y a) \end{aligned} \quad (1)$$

where t and t_i ($i = 1, 2, 3, 4$) are hopping parameters. Their relative ratios are $t_1/t = -0.136$, $t_2/t = 0.068$, $t_3/t = 0$, $t_4/t = -0.02$, and $t = 1720$ meV. Fermi-surface changes with doping are achieved by tuning the chemical potential, μ , while keeping the hopping parameters unchanged.

SUPPLEMENTARY NOTE 2: FITTING OF THE CDW PEAK

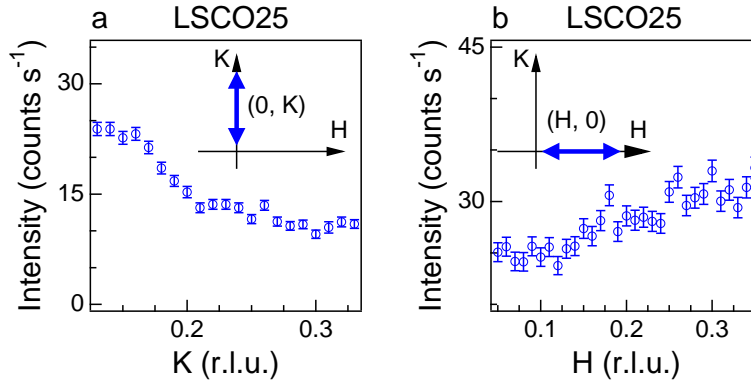
Following previous studies [3, 5–7], the CDW peaks were fitted by a Lorentzian-squared function

$$I_{\text{CDW}}(T) = I_{\text{BG}}(T) + \frac{I_0(T)}{\left(1 + \left[\frac{Q - Q_0(T)}{\Gamma}\right]^2\right)^2} \quad (2)$$

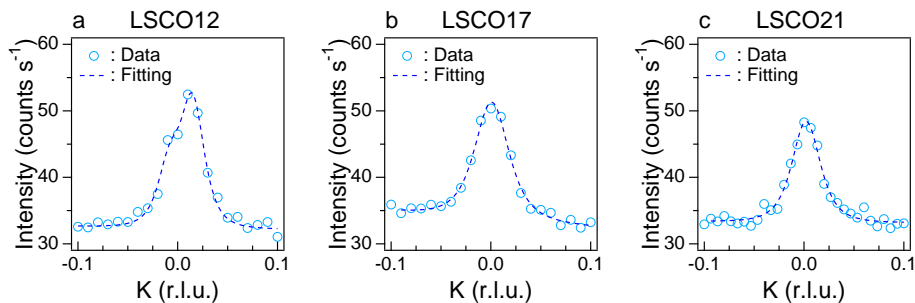
where $I_{\text{BG}}(T)$ is a polynomial background, which we found to be of third order in the present dataset. The relation between Γ , (HWHM), and in-plane correlation length, ξ_{\parallel} , is given by $\text{HWHM} = \Gamma \sqrt{(\sqrt{2} - 1)}$ where $\Gamma = 1/\xi_{\parallel}$. In Fig. 2 of the main text, we show representative fittings for scans along \mathbf{Q}_{CDW} (longitudinal scans). Representative fittings for scan perpendicular to \mathbf{Q}_{CDW} (transverse scan) are shown in Supplementary figure 2. We used two Lorentzian-squared peaks to fit transverse scans in LSCO12 due to the known splitting of CDW peaks are known to split at this concentration [3, 4]. The HWHMs that are extracted from different transverse and longitudinal scans agree within 5% with respect to averaged value.

SUPPLEMENTARY NOTE 3: ABSENCE OF CDW SIGNAL IN LSCO25

Supplementary figure 1 shows K and H of LSCO25 scans near possible CDW wavevectors. Within our experimental uncertainty, we do not observe any CDW superlattice peaks at $T = 15$ K $\approx T_{\text{SC}}$. This was observed consistently



Supplementary figure 1. Absence of a CDW peak in LSCO25. (a) and (b) shows scans along the K and H directions, respectively. The scans are taken at $L = 12.5$. The in-plane scan trajectories are shown as insets to each panel. The data were taken at 15 K, just above T_{SC} . Errorbars are one standard deviation based on Poissonian statistics.



Supplementary figure 2. Fitting of the CDW peak. Representative Lorentzian-squared fits (Eq. 2 of the CDW peak perpendicular to \mathbf{Q}_{CDW} near T_{SC} are shown in (a)-(c). Note that the data for LSCO12 is composed of two peaks, as previously demonstrated [3, 4]. Errorbars are one standard deviation based on Poissonian statistics.

with different samples and different beamlines. The absence of a CDW points towards a possible connection between CDW correlations and non-Fermi-liquid transport as both seem to disappear concurrently (see also Appendix V) .

SUPPLEMENTARY NOTE 4: CDW INTENSITY

Assuming a weak interplanar CDW correlation, the integrated x-ray scattering intensity, $I^{\text{int}} = I_0 \text{HWHM}^2 = I^{\text{peak}}(\sqrt{2} - 1)\Gamma^2$, is used to estimate the magnitude of the CDW order parameter [8]. Former x-ray studies found that the CDW magnitude in LSCO12 is about four times smaller than in $\text{La}_{1.875}\text{Ba}_{0.125}\text{CuO}_4$ and $\text{YBa}_2\text{Cu}_3\text{O}_{6.612}$ (YBCO) [8]. This is based on a direct comparison of scattering intensity in reflection using 9 keV x-rays. We note that LSCO has a shorter x-ray penetration depth of between 6.70-6.9 μm (dependent on doping) compared to 8.2 μm in YBCO. We remind the reader that LSCO also has fewer CuO_2 planes per unit volume compared to YBCO, such that approximately three times fewer CuO_2 planes are illuminated in LSCO compared to YBCO. In this study, we use the same LSCO12 sample as previously [3]. The comparable CDW peak intensity and correlation length confirms that the CDW order parameter is of substantial size throughout the phase diagram (see Fig. 4 of the main text) and is expected to have an appreciable effect on the transport properties.

As we discussed in the main text, I^{int} also varies with doping. Based on the fits shown in Supplementary figure 3 of the main text, we find intensity ratios of 8:7:1 at T_{SC} for $x = 0.12, 0.17,$ and 0.21 . The magnitudes of the CDW order parameter are estimated based on data at $T = T_{\text{SC}}$. The appreciable reduction of I^{int} in LSCO21 occurs close to the crossover from strange metal to Fermi liquid phase at low temperature.

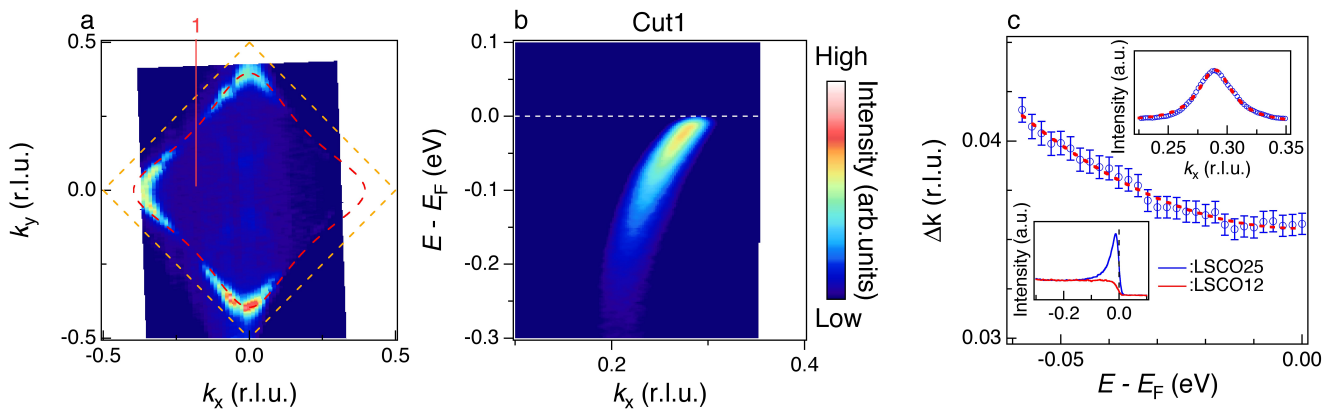
SUPPLEMENTARY NOTE 5: RECOVERY OF QUASI-PARTICLE COHERENCE IN LSCO25

The ARPES intensity map of LSCO25 at E_F is shown in Supplementary figure 3(a). In agreement with previous studies [2, 9], well-defined quasiparticles are recovered in this heavily overdoped sample as shown in Supplementary figure 3(b)&(c). Near E_F , the quasiparticle scattering rate is given by $\text{Im}\Sigma(k, \omega) = \frac{1}{2}\hbar v_F \Delta k(\omega)$, where $\text{Im}\Sigma(k, \omega)$ is the imaginary part of the self-energy, v_F and ω are the Fermi velocity and the binding energy, respectively [10]. $\Delta k(\omega)$ can be extracted by fitting the momentum distribution curve (MDC) with a Lorentzian function

$$\Gamma^{\text{MDC}}(k, \omega) = I_{\text{BG}} + \frac{I_0(\omega)}{(k - k_0)^2 + (\Delta k)^2}, \quad (3)$$

where $I_{\text{BG}}(\omega)$ and $I_0(\omega)$ are constants at fixed ω . Supplementary figure 3(c) shows the extracted $\Delta k(\omega)$, which can be further fitted with $a + b\omega^2$, as expected for a Fermi-liquid. One can also directly observe the emergence of a coherent quasiparticle peak the LSCO25 energy distribution curve (EDC) that was not present when compared to an LSCO12 EDC at a nearby E_F .

[1] Horio, M. *et al.* Three-dimensional Fermi surface of overdoped La-based cuprates. *Phys. Rev. Lett.* **121**, 077004 (2018).



Supplementary figure 3. The electronic structure of LSCO25. (a) ARPES intensity map at E_F obtained by integrating the spectra in a ± 10 meV energy window with respect to E_F . (b) Band dispersion along the red line shown in (a). (c) Display fits to the energy and momentum distribution curves (MDCs/EDCs). The upper panel shows the MDC (blue points) and a fit to a Lorentzian-function (Eq. 3) (red dashed curve) at E_F . The extracted MDC-width, Δk , is plotted as function of energy in the main panel of (c), which shows a ω^2 -dependence, which is consistent with Fermi liquid behavior. The red-dashed curve shown in the main panel of (c) is a fit of the extracted Δk using a quadratic function, $a + b^2$. The bottom-left panel compares EDCs of LSCO12 (red) and LSCO25 (blue) at representative k_F , which are close in momentum space. Errorbars are one standard deviation derived from least-squares fitting.

- [2] Chang, J. *et al.* Anisotropic breakdown of fermi liquid quasiparticle excitations in overdoped $\text{La}_{2-x}\text{Sr}_x\text{CuO}_4$. *Nat. Commun.* **4**, 1–5 (2013).
- [3] Thampy, V. *et al.* Rotated stripe order and its competition with superconductivity in $\text{La}_{1.88}\text{Sr}_{0.12}\text{CuO}_4$. *Phys. Rev. B* **90**, 100510 (2014).
- [4] Wen, J.-J. *et al.* Observation of two types of charge-density-wave orders in superconducting $\text{La}_{2-x}\text{Sr}_x\text{CuO}_4$. *Nat. Commun.* **10**, 3269 (2019).
- [5] Wilkins, S. B. *et al.* Comparison of stripe modulations in $\text{La}_{1.875}\text{Ba}_{0.125}\text{CuO}_4$ and $\text{La}_{1.48}\text{Nd}_{0.4}\text{Sr}_{0.12}\text{CuO}_4$. *Phys. Rev. B* **84**, 195101 (2011).
- [6] Chen, X. M. *et al.* Remarkable stability of charge density wave order in $\text{La}_{1.875}\text{Ba}_{0.125}\text{CuO}_4$. *Phys. Rev. Lett.* **117**, 167001 (2016).
- [7] Miao, H. *et al.* High-temperature charge density wave correlations in $\text{La}_{1.875}\text{Ba}_{0.125}\text{CuO}_4$ without spin-charge locking. *Proc. Natl. Acad. Sci. U.S.A.* **114**, 12430–12435 (2017).
- [8] Thampy, V. *et al.* Comparison of charge modulations in $\text{La}_{1.875}\text{Ba}_{0.125}\text{CuO}_4$ and $\text{YBa}_2\text{Cu}_3\text{O}_{6.6}$. *Phys. Rev. B* **88**, 024505 (2013).
- [9] Yoshida, T. *et al.* Electronlike fermi surface and remnant $(\pi, 0)$ feature in overdoped $\text{La}_{1.78}\text{Sr}_{0.22}\text{CuO}_4$. *Phys. Rev. B* **63**, 220501 (2001).
- [10] Valla, T. *et al.* Evidence for quantum critical behavior in the optimally doped cuprate $\text{Bi}_2\text{Sr}_2\text{CaCu}_2\text{O}_{8+\delta}$. *Science* **285**, 2110–2113 (1999).